Field patterns of pulsed, focused, ultrasonic radiators in attenuating and nonattenuating media

Mitchell M. Goodsitt, Ernest L. Madsen, and James A. Zagzebski

Medical Physics Department, University of Wisconsin, Room 1530, 1300 University Avenue, Madison, Wisconsin 53706
(Received 17 July 1981; accepted for publication 1 November 1981)

A theoretical method which can be used to calculate the pressure field patterns of pulsed, focused, ultrasonic radiators in attenuating and nonattenuating media is discussed in this paper. The underlying principle involved is the superposition of continuous wave beams to form pressure pulses. The method is adapted to the circumstances associated with using a hydrophone to measure field patterns. Experimentally obtained hydrophone signals are then compared to theoretical predictions. The field patterns of four transducer-pulser combinations are investigated. A medium with tissue-mimicking acoustical properties is used to attenuate the ultrasonic beam in these studies. The theory compares favorably with experiment whether an attenuating medium is present or not. However, the theory fails at positions very close to the transducer face (~ 1 cm) and when significant nonlinear effects occur during the transmission of the pulse through the medium. This work may have significant applications in research devoted to designing ultrasonic transducers for particular studies, determining dose profiles of medical ultrasonic machines, and analyzing the ultrasonic signals backscattered from within patients.

PACS numbers: 43.20.Rz, 43.20.Px, 43.35.Yb, 43.20.Hq

INTRODUCTION

Presently, the majority of the radiators or transducers that are employed in medical diagnostic ultrasound are focused and operated in the pulsed mode. The ability to predict, theoretically, the field patterns of the beams emitted by such transducers is of fundamental importance in many areas of medical ultrasound research. Field pattern information can be used to aid in the design of pulser-transducer combinations for imaging specific organs within the human body. Accurate predictions of the average and temporal peak intensities in the beam are valuable in dosimetric and bioeffects studies. In addition, the ability to predict the pressure waveforms at different positions within the beam may be useful in the development of ultrasonic signal analysis schemes.[1] The most relevant situation associated with the above applications is that of a pulsed, focused transducer transmitting into an attenuating medium closely simulating soft tissue. While the pressure field patterns of pulsed, nonfocused transducers in nonattenuating media have been the subject of many theoretical investigations,[2-18] the literature is almost void of theoretical articles about these patterns for pulsed, focused radiators.[19] To our knowledge, no theoretical descriptions have been published for such patterns in attenuating media.

In order to learn about the general characteristics of ultrasonic beams, simulated pulses were commonly introduced into the theoretical models for the pressure field patterns in nonattenuating media. For example, in their models for pulsed, nonfocused radiators in nonattenuating media, Bardsley and Christensen[18] employed exponentially damped sinusoidal pulses, Weyns[17] employed sine-modulated Gaussian pulses, and Weight and Hayman,[15] Robinson,[12] and Beaver[13] employed half sine wave monopulses. Furthermore, Weyns[19] employed sine-modulated Gaussian pulses in his model for a pulsed, focused radiator in nonattenuating media. The only comparison between theory and experiment was published by Weight and Hayman.[15] This was for the case of a pulsed, nonfocused transducer operating in a nonattenuating medium. The experimental pulse in their study was created to match the theoretical simulation, and only on-axis field patterns were compared. Although simulations such as those described above yield valuable information about ultrasonic beams, the pressure fields in actual clinical situations, that is, in attenuating media with real pulses, may have significantly different characteristics.

Superposition theory yielding pressure field patterns of pulsed, focused radiators in attenuating and nonattenuating media was outlined in a companion article.[20] In this paper, this theory is applied to calculate the signals which a hydrophone pressure receiver should output when it is placed at any position within the ultrasonic field of a pulsed, focused transducer. An experimental signal recorded by the hydrophone at one position in the beam of the transducer is introduced into the theory to predict the signals at other hydrophone positions. The theoretical signals are compared with those observed experimentally when a nonattenuating medium is present between the transducer and the hydrophone, and when a slab of tissue-mimicking, attenuating material with known acoustical properties, in the form of a phantom, displaces some of the nonattenuating medium between the transducer and the hydrophone. Two medical, focused, ultrasonic transducers are studied for the cases in which they are driven by a clinical pulser and a laboratory model pulser.

The very important fact that theory and experiment are compared throughout this work allows subtle aspects as well as limitations of the theoretical model to be studied. The consequences of employing various frequency dependency relations for the speed of sound in the theory are investigated. Also, the influences of nonlinear effects in the transmission medium and the theoretical prediction of "edge waves"[2,3] are explored.

 0001-4966/82/020318-12$00.80

I. IMPLEMENTATION OF THE THEORY

A. The pulsed pressure field in attenuating and nonattenuating media

The transducer of interest may be described as a concave, dome-shaped portion of a spherical radiator. The radiating element is modeled as a set of equivalent monopole sources uniformly distributed over the face of the radiator. These sources are assumed to vibrate in phase.

The continuous wave (cw) pressure distribution of such a radiator may be approximated by the Rayleigh function which is in the form of an integral over the area of the transducer face.[21] This involves the evaluation of a double integral. An equivalent single integral expression for the cw pressure distribution was derived in a companion article.[20] It was also shown in that article that the attenuating and dispersive effects associated with transmission of the ultrasonic beam through an attenuating material can be introduced into the theory via the complex wavenumber $k_c = [\omega/c(\omega)] + i\alpha(\omega)$, where ω is the angular frequency, $c(\omega)$ is the speed of sound as a function of angular frequency, $i = (-1)^{1/2}$ and $\alpha(\omega)$ is the attenuation coefficient as a function of angular frequency. When $\alpha(\omega)$ is negligible for all ω, k_c reduces to its unattenuated value (k) of ω/c. Introducing the complex wavenumber into the single integral for the cw pressure distribution, the pressure amplitude at field point $\mathbf{r}$ as a function of ω becomes

$$P(\mathbf{r},\omega) = \frac{-\rho u_0 \omega A}{\pi k_c s} \cdot \left(ik_c \int_{C'}^{D'} \beta(r') e^{ik_c r'} dr' + F \right). \quad (1)$$

where

$$C' = [A^2 + s^2 + 2As\cos(\psi_u + \phi)]^{1/2},$$

$$D' = [A^2 + s^2 + 2As\cos(\psi_u - \phi)]^{1/2},$$

$$\beta(r') = \cos^{-1}\left(\frac{h + (A^2 - a^2)^{1/2} - (r'^2 + s^2 - A^2/2s)\cos\phi}{(\sin\phi/2s)[4s^2 r'^2 - (r'^2 + s^2 - A^2)^2]^{1/2}} \right),$$

$$F = \begin{cases} 0, & \text{for } |x/h| \geq a/A \text{ (region 2)}, \\ \dfrac{\pi|h|}{h}\left(\exp\left[ik_c\left(A + \dfrac{hs}{|h|} \right) \right] - \exp\left\{ ik_c\left[A^2 + s^2 + 2As\cos\left(\psi_u - \dfrac{h}{|h|}\phi \right) \right]^{1/2} \right\} \right), & \text{for } \left|\dfrac{x}{h}\right| < \dfrac{a}{A} \text{ (region 1)}, \end{cases}$$

and a = projected transducer radius, A = radius of curvature of transducer, $\mathbf{r} = (x,z)$, $h = z - A$, $s = (x^2 + h^2)^{1/2}$, $\phi = \tan^{-1}(x/h)$, $\psi_u = \sin^{-1}(a/A)$, ρ = density of the medium through which the pressure wave travels, and u_0 is the velocity amplitude at the surface of the radiator. The coordinates and the regions for F are displayed in Fig. 1. The pressure field is assumed to be cylindrically symmetric about the z axis. As is indicated in Eq. (1), a single integral is still applicable in the attenuated case.

The pressure pulse emitted by an ultrasonic transducer may be expressed as a linear superposition of continuous wave beams varying sinusoidally in time. A complete set of continuous wave beams at a field point $\mathbf{r}$ can be represented mathematically by the set of terms $P_N(\mathbf{r},\omega)e^{-i\omega t}$ for all ω, $0 \leq \omega < \infty$. Here, the $P_N(\mathbf{r},\omega)$ are normalized versions of the $P(\mathbf{r},\omega)$ in Eq. (1). They can, for example, be obtained by setting the $\rho(u_0/\pi)$ term in this equation equal to 1. To calculate the pressure as a function of time at the field point for a pulsed transducer, each continuous wave beam, $P_N(\mathbf{r},\omega)e^{-i\omega t}$, must be weighted by a corresponding complex amplitude $A_0(\omega)$ specific to the particular pulse, and the results superimposed. This may be expressed as

$$p(\mathbf{r},t) = \mathrm{Re}\left(\int_0^\infty P_N(\mathbf{r},\omega) A_0(\omega) e^{-i\omega t} d\omega \right), \quad (2)$$

where Re denotes "real part of."

Equivalently, we can write

$$p(\mathbf{r},t) = \int_{-\infty}^{\infty} P_N(\mathbf{r},\omega) A_0(\omega) e^{-i\omega t} d\omega, \quad (3)$$

where the P_N's and A_0's for negative frequencies are given by

$$P_N(\mathbf{r},-\omega)A_0(-\omega) = P_N^*(\mathbf{r},+\omega)A_0^*(+\omega)$$

(* denotes complex conjugation). Also, a factor of 1/2 has been absorbed in the $A_0(\omega)$ term in Eq. (3).

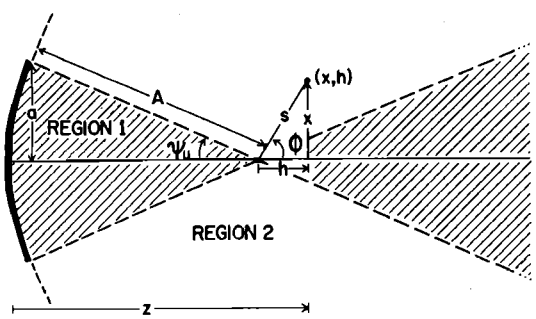

FIG. 1. Diagram depicting the regions, coordinates, and some of the parameters associated with Eq. (1). Note $-A \leq h < \infty$.

B. Hydrophone response

Experimental determinations of the field patterns of ultrasonic transducers are commonly made using miniature pressure receivers such as hydrophones. Application of the theory to the case of a hydrophone receiver necessitates several adaptations. Both the finite size of the pressure-sensitive element of the hydrophone and the voltage nature of the output signal of the hydrophone must be considered.

We model the hydrophone as a circular, planar, piston receiver with zero time delay transient response.

It should be emphasized that the nonzero diameter of the receiving element means that the hydrophone response to a pulse is, at best, proportional to the net force on this receiving element as a function of time, and this is true only if the input force to output voltage transfer function of the hydrophone is frequency independent. Also, the instantaneous pressure in different regions of the receiving element can vary considerably; thus, even for a frequency independent transfer function, the instantaneous net force is not in general proportional to the pressure at some reference point such as the center of the hydrophone receiving element. The effect of the nonzero size of the hydrophone is accounted for in our model by partitioning the (modeled) receiving element into annular rings or segments thereof, and numerically integrating the instantaneous pressure over the receiver area.

The force-to-voltage transfer function of the hydrophone is generally at least a slowly varying function of frequency; hence, in the pulsed wave case, there is no simple proportionality between the hydrophone output voltage signal and the instantaneous net force on the hydrophone face. Rather, they are related as follows:

$$s(\mathbf{r}_c, t) = \int_{-\infty}^{\infty} F_N(\mathbf{r}_c, \omega) A_0(\omega) T(\omega) e^{-i\omega t}\, d\omega \tag{4}$$

or

$$s(\mathbf{r}_c, t) = \int_{-\infty}^{\infty} F_N(\mathbf{r}_c, \omega) H(\omega) e^{-i\omega t}\, d\omega ,$$

where $s(\mathbf{r}_c, t) \equiv$ voltage signal as a function of time t when the center of the hydrophone receiving element is positioned at field point $\mathbf{r}_c$.

$$F_N(\mathbf{r}_c, \omega) \equiv \int_{\text{hydrophone face}} P_N(\mathbf{r}, \omega)\, dA'$$

$$= \text{net force on the hydrophone face.}$$

The $P_N(\mathbf{r}, \omega)$ are obtained from Eq. (1), and dA' = area element on the hydrophone face. $A_0(\omega)\, d\omega \equiv$ complex amplitude of the ω spectral component of the pressure pulse. $T(\omega) \equiv$ force-to-voltage transfer function of the hydrophone, and $H(\omega) \equiv A_0(\omega) T(\omega)$.

In order to use Eq. (4) to calculate theoretical voltage signals, the hydrophone modified spectral content of the pulse, $H(\omega)$, must first be determined. A technique that can be used to determine the $H(\omega)$ involves placing the hydrophone at any position within the ultrasonic beam, obtaining a reference signal $s_{\text{ref}}(\mathbf{r}_c, t)$, and then solving the inverse Fourier transform counterpart of Eq. (4) for the $H(\omega)$. That is,

$$H(\omega) = \left(\frac{1}{2\pi} \int_{-\infty}^{\infty} s_{\text{ref}}(\mathbf{r}_c, t) e^{i\omega t}\, dt \right) \Big/ F_N(\mathbf{r}_c, \omega) . \tag{5}$$

It is important to realize that once the $H(\omega)$ are known, theoretical hydrophone output voltage signals can be calculated for any hydrophone position within the beam of the pulsed, focused transducer by using Eq. (4). Also, if in addition to the $H(\omega)$, the force-to-voltage transfer function, $T(\omega)$, of the hydrophone is known (e.g., as a result of calibrated force balance measurements), theoretical and experimental force signals can be compared. The theoretical force signal $f(\mathbf{r}_c, t)$ is calculated by using the equation

$$f(\mathbf{r}_c, t) = \int_{-\infty}^{\infty} F_N(\mathbf{r}_c, \omega) \frac{H(\omega)}{T(\omega)} e^{-i\omega t}\, d\omega . \tag{6}$$

The experimental force signal is obtained by calculating the Fourier transform, $S(\mathbf{r}_c, \omega)$, of the experimental voltage signal, $s(\mathbf{r}_c, t)$, and inserting it into the equation

$$f_{\text{exp}}(\mathbf{r}_c, t) = \int_{-\infty}^{\infty} \frac{S(\mathbf{r}_c, \omega)}{T(\omega)} e^{-i\omega t}\, d\omega . \tag{7}$$

C. Particular experimental considerations

1. Geometry of the attenuating medium

The arrangement that was used to obtain the experimental data reported in this paper is shown in Fig. 2. A hydrophone was employed to respond to the pressure field. The attenuating media were in the form of cylindrical phantoms occupying only part of the region between the hydrophone and the transducer face. To account for this shape influence, effective speeds of sound and attenuation coefficients were computed and introduced into the theory. The pertinent parameters for the effective value calculations are depicted in Fig. 2. z_c and x_c are, respectively, the axial and lateral positions of the center of the hydrophone face and D is the thickness of the cylindrical phantom, the flat parallel end faces of the cylinder being vertical and perpendicular to the figure. The length of the straight line between the center of the transducer face and the center of the hydrophone face is chosen as an effective pathlength. The effective attenuation coefficient is defined to be

$$\alpha_e(\omega) \equiv \alpha(\omega)(D/z_c) , \tag{8}$$

where $\alpha(\omega)$ is the (measured) attenuation coefficient of the phantom material.

The effective speed of sound is defined to be

$$c_e(\omega) = \frac{z_c}{[(z_c - D/\cos\theta)/c_0] + [(D/\cos\theta)/c(\omega)]} , \tag{9}$$

where c_0 is the (measured) speed of sound in the alcohol–water mixture in which the transducer, hydrophone, and phantom are submerged and $c(\omega)$ is the (measured) speed of sound of the phantom material.

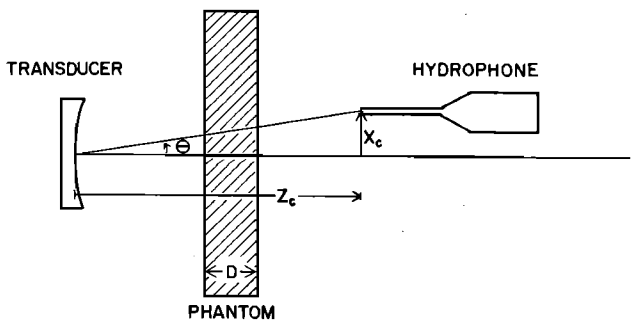

FIG. 2. A typical off-axis situation analyzed in the experimental studies of this paper. (x_c, z_c) is the center of the receiving element of the hydrophone. Parameters in this figure are employed in the effective attenuation coefficient and speed of sound calculations.

Values obtained with these expressions are good approximations to those that would be obtained along paths between area elements on the transducer face and the center of the hydrophone face, and the expressions simplify calculations considerably.

2. *Discrete sampling*

The majority of the equations in the hydrophone response section of this paper (Sec. IB) are in the form of Fourier transforms. In the experiment that was performed, individual hydrophone output signals were discretely sampled and digitized. As a consequence, the above-mentioned equations were evaluated using fast Fourier transforms. The sampling theorem criteria[22,23] were fulfilled to avoid aliasing effects. That is, for 1024 samples of the hydrophone output signal, each separated by 0.01 μs, the frequency components in the calculations were each separated by $1/(1024 \times 0.01 \times 10^{-6})$ Hz.

II. MEASUREMENT PROCESS

A. Setup

The complete experimental setup is depicted in Fig. 3. The $26 \times 28 \times 57$-cm scanning tank was filled with an alcohol–distilled water mixture with a speed of sound within 3 m/s of that of the attenuating media in the phantoms (~1570 m/s). This minimized refractive effects. Two Aerotech medical ultrasonic transducers were employed in the experiments—a 3.5-MHz, 19-mm diam, long internal focus transducer, the same one that was used in the accompanying article, and a 2.25-MHz, 19-mm diam, long internal focus transducer. Two different pulsers were employed in this study. One, a Panametrics 5052, used an SCR discharge circuit to deliver a fast rise time voltage pulse to the transducers. The second delivered a current pulse to the transducers and was part of a Unirad Sonograph II commercial B-scan instrument. This Unirad unit is about eight years old. Hereafter, the Panametrics and Unirad pulsers will be referred to as pulsers "P" and "U," respectively. The hydrophone that was used was a Raytheon PVF_2 polymer prototype with an active (receiving) element diameter of 1.5 mm. This probe was specifically designed for mapping the pressure fields emitted by ultrasonic transducers.[24] Its transient response compares favorably to that of a laser pellicle pressure detection system.[24] The remainder of the setup consisted of an x–y–z translator which was used to position the center of the hydrophone face at any field point within the ultrasonic beam, a Biomation 8100 transient recorder which digitized with 8-bit resolution at a 100-MHz rate the signal output by the hydrophone, and a Digital Equipment Corporation PDP 11/34 minicomputer which was programmed to calculate the theoretical signals and display both the theoretical and experimental signals. The x,y,z coordinate directions are displayed at the bottom of Fig. 3.

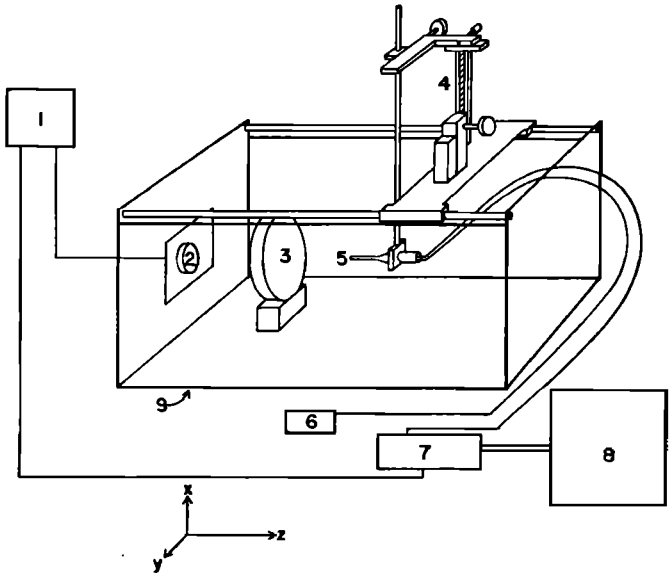

FIG. 3. Components of the experimental setup. 1 represents the pulser; 2 the focused transducer; 3, the attenuating medium phantom; 4, the x–y–z translator; 5, the hydrophone; 6, the hydrophone pre-amp power supply; 7, the transient recorder, 8, the minicomputer; and 9, the scanning tank.

B. Alignment of the axes

The transducer-hydrophone system was aligned by following the procedure outlined below.

(1) The hydrophone receiving element was positioned in the alcohol/water mixture at the approximate center of curvature of the transducer.

(2) Pulser P was used to drive the transducer, and the hydrophone was translated vertically and horizontally to find the x–y position at which its output signal was a maximum.

(3) The hydrophone receiving element was then moved in the $+z$ direction (see Fig. 1 or 2) to a new position approximately 10 cm further from the transmitting transducer.

(4) The hydrophone was again translated vertically and horizontally to find the x and y positions of the peak detected signal.

(5) If either the x values in steps 2 and 4 or the y values in steps 2 and 4 differed by more than 0.3 mm, the direction of the transducer was adjusted, and the entire process was repeated.

When, finally, all x,y position discrepancies were less than or equal to ± 0.3 mm, the z-translation axis and the transducer beam "center" were aligned to within $\pm 0.2°$.

C. Positioning of hydrophone for recording experimental signals

For the recording of the receiver voltage signals, the hydrophone was positioned axially by (1) calculating the transit time in the alcohol–water mixture for the desired axial distance, (2) setting the trigger delays on the Biomation transient recorder to correspond to this transit time, and (3) translating the hydrophone on-axis to the position at which the front of the voltage signal output by the hydrophone and digitized by the transient

recorder was displayed at the beginning of the transient recorder D/A output. Axial positions determined in this manner were accurate to within ±0.3 mm. Lateral positioning of the hydrophone was accomplished by using the scales on the $x-y-z$ translator. The errors associated with the lateral positions were approximately ±0.1 mm.

D. Tissue-mimicking materials and details of phantom structure

The phantoms used were lucite cylinders filled with tissue-mimicking (TM) material.[25] The inner diameter of the cylinders was 7.6 cm, and the ends were covered with 10 μ thick saran wrap. Thus the TM material was separated at both ends from the alcohol–water solution by thin (10 μ thick) transmission windows. The TM material consists of gelatin in which microscopic graphite particles are suspended. These particles determine the attenuation characteristics.

The frequency dependent speed of sound and attenuation coefficient of the TM phantom material were measured at nine frequencies between 0.7 and 12 MHz using a substitution technique.[24] Applying regression routines to the attenuation data resulted in the following relationship:

$$\alpha(f) = (1.32\ \text{dB/cm/MHz})f + 0.00145\ \text{dB cm}^{-1}\ \text{MHz}^{-3.7} f^{3.7}. \quad (10)$$

Using Eq. (10) and the application of the Kramers–Kronig relationship to ultrasound,[26] a frequency-dependent speed of sound was derived. For frequencies greater than 2 MHz, the measured speed of sound data deviated from that calculated using the Kramers–Kronig relation. Following is a polynomial fit to this measured data:

$$c(f) = (1570.27 + 1.456\ \text{MHz}^{-1} f - 0.136\ \text{MHz}^{-2} f^2)\text{m/s}. \quad (11)$$

E. Determination of A and a

As is apparent from Eq. (1), the theory requires a knowledge of two-dimensional characteristics of the transducer: the radius of curvature, A, and the projected radius, a. The radius of curvature of each transducer was experimentally determined in the same manner as in the companion article.[20] The method is based upon O'Neil's theoretical result[21] that the relative pressure in the focal plane at angle θ from the axis is, to a very good approximation, given by the directivity function $2J_1(ka \sin\theta)/ka \sin\theta$, where J_1 is a Bessel function of the first kind, and k and a are as previously defined. It follows that the center of curvature of the transducer could be determined by finding the axial distance at which, for gated bursts of continuous wave excitation of the transducer, the closest approximation to the shape of the absolute value of a directivity function is output by the hydrophone (peak-to-peak voltage) as it is translated laterally in the unattenuated beam. The radius of curvature would then be equal to this axial distance. Using this method at a cw frequency of 2.46 MHz, the radius of curvature of the 3.5-MHz transducer was found to be 11.0 ±0.1 cm and that of the 2.25-MHz transducer to be 13.7 ±0.1 cm. The projected radius of each transducer was also determined experimentally by finding the polar angle θ at which the first zero of the directivity function approximation output by the hydrophone occurred. When this value and the wavenumber k of the continuous wave burst were inserted into the equation for the first zero of J_1, the solution for the projected radius was obtained ($a = 3.83/k \sin\theta$). For the 3.5-MHz transducer, a was found to be 9.4 mm, and for the 2.25-MHz transducer, a was found to be 9.14 mm. The transducer manufacturer quotes a value of 9.5 mm for both transducers. The discrepancies may be due to apodization; that is, due to the fact that the transducers' active elements were constrained at their outer edges.

III. RESULTS

This section is devoted to a comparison between theoretical and experimental hydrophone waveforms. The influences of field position in the ultrasonic beam, attenuating conditions, and spectral content of the pulses are investigated.

Before proceeding with the theoretical and experimental comparisons, some specific information related to these comparisons should be discussed. First, theoretical predictions of hydrophone voltage signals rather than force signals were compared to their experimental counterparts. This resulted in an adequate test of the model without the necessity of acquiring accurate measurements of the force-to-voltage transfer

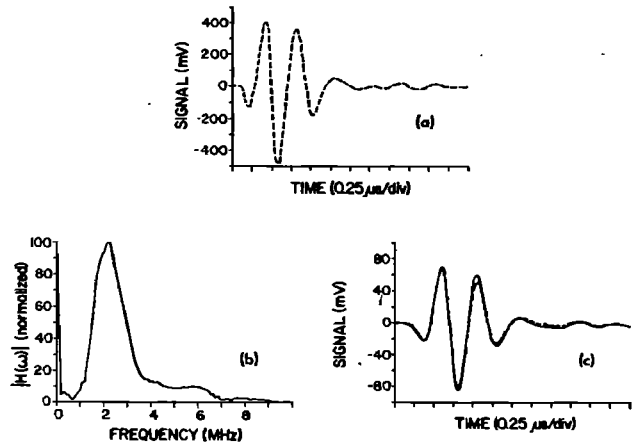

FIG. 4. 2.25-MHz transducer-pulser P results at $z_c = 8$ cm. (a) Reference signal output by the hydrophone when the center of its active element was positioned in the H_2O/alcohol mixture (unattenuated), on-axis ($x_c = 0$ mm, $y_c = 0$ mm) at $z_c = 8$ cm. (b) Normalized modulus of the hydrophone modified spectral content of the pulse. The $H(\omega)$ are used in the calculations to predict the theoretical signals. (c) Comparison between theory (solid line) and experiment (broken line) for the signal obtained when the center of the hydrophone active element was positioned on-axis at $z_c = 8$ cm and a 5 cm thick phantom of 1.32-dB/cm/MHz attenuating material was placed between the transducer and the hydrophone face. The ratio of the peak-to-peak theoretical signal voltage to the peak-to-peak experimental signal voltage is (V_{pp} theory to exp. ratio) 1.06. The ratio of the rms theoretical signal voltage to the rms experimental signal voltage is (V_{rms} theory to exp. ratio) 1.086.

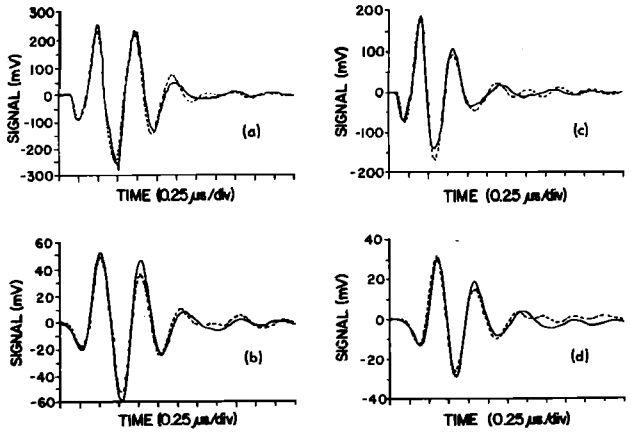

FIG. 5. 2.25-MHz transducer-pulser "P" results at $z_c = 5.2$ cm. Theory = solid line, experiment = broken line. (a) On-axis, unattenuated; (b) on-axis, attenuated with a 5 cm thick phantom (1.32 dB/cm/MHz); (c) off-axis ($x_c = 4$ mm, $y_c = 0$ mm, $z_c = 5.2$ cm), unattenuated, and (d) off-axis ($x_c = 4$ mm, $y_c = 0$ mm, $z_c = 5.2$ cm), attenuated with 5 cm thick phantom (1.32 dB/cm/MHz). V_{pp} theory to exp. ratio = 1.143, 1.122, 0.910, 1.043 in (a), (b), (c), and (d), respectively. V_{rms} theory to exp. ratio = 1.016, 1.142, 0.960, 1.060 in (a), (b), (c), and (d), respectively.

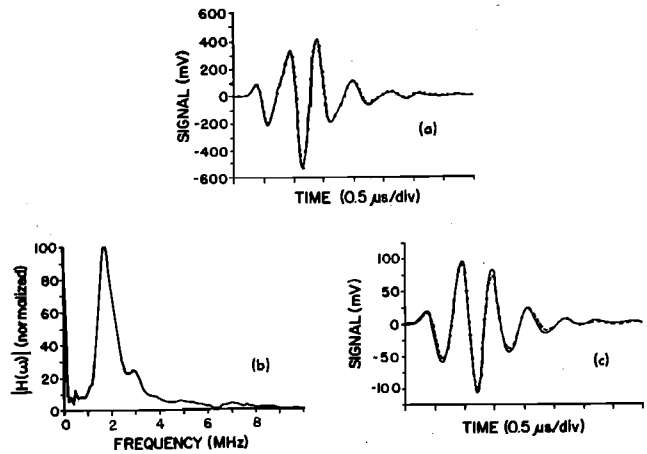

FIG. 7. 2.25-MHz transducer-pulser U results at $z_c = 8$ cm. (a) Reference signal—unattenuated, recorded on-axis at $z_c = 8$ cm; (b) $|H(\omega)|$ versus frequency for the reference signal. The corresponding $H(\omega)$ are used to calculate the theoretical 2.25-MHz transducer-pulser U signals. (c) Theory (solid line) versus experiment (broken line) on-axis at $z_c = 8$ cm with 5 cm thick phantom (1.32 dB/cm/MHz) between the transducer and hydrophone. V_{pp} theory to exp. ratio = 1.067. V_{rms} theory to exp. ratio = 1.084.

function of the hydrophone at all of the frequencies associated with the pulse. Second, related to the fact that the receiver characteristics were not precisely known (i.e., the hydrophone was likely not simply a flat circular piston of zero response time and known radius), it was assumed that the best experimental determination of the hydrophone modified spectral content of the pulse, $H(\omega)$, could be obtained if the hydrophone position were chosen so as to minimize the effects of phase variation across its face. Either a position in the focal region (region of peak pressure amplitude) or at the center of curvature of the transducer was chosen. Best agreement between theory and experiment resulted when the $H(\omega)$ was determined from reference signals output by the hydrophone when it was placed in the focal region of the transducer. Finally, the reader is reminded that the theoretical signals were obtained by numerical integration over the hydrophone face. In doing this integration, the hydrophone face was divided into four area segments. A precision check using eight

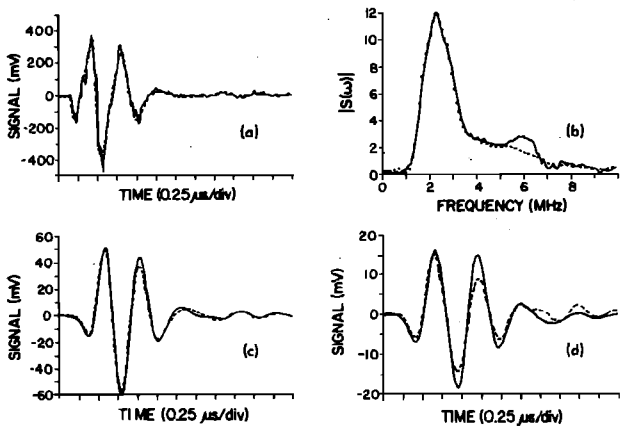

FIG. 6. 2.25-MHz transducer-pulser P results at $z_c = 13.7$ cm. Theory = solid line, experiment = broken line. (a) On-axis, unattenuated; (b) moduli of the Fourier transforms of the experimental and theoretical signals in (a); (c) on-axis, attenuated with 5 cm thick phantom (1.32 dB/cm/MHz); and (d) off-axis ($x_c = 5$ mm, $y_c = 0$ mm, $z_c = 13.7$ cm), attenuated with 5 cm thick phantom (1.32 dB/cm/MHz). V_{pp} theory to exp. ratio = 1.180, 1.038, 1.189 in (a), (c), and (d), respectively. V_{rms} theory to exp. ratio = 1.019, 1.060, 1.267 in (a), (c), and (d), respectively.

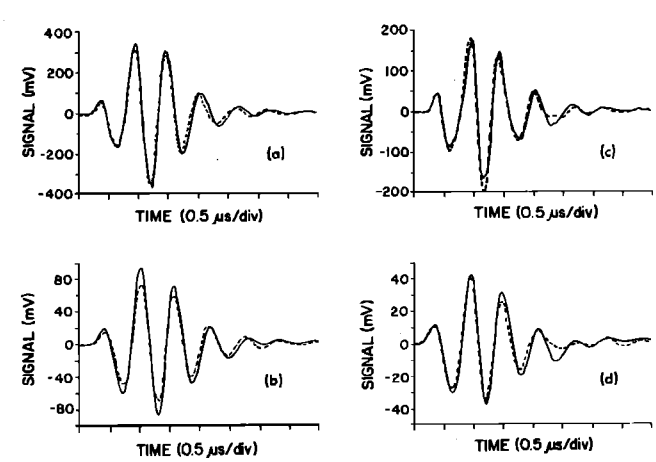

FIG. 8. 2.25-MHz transducer-pulser U results at $z_c = 5.2$ cm. Theory = solid line, experiment = broken line. (a) On-axis, unattenuated; (b) on-axis, attenuated with 5 cm of 1.32 dB/cm/MHz; (c) off-axis ($x_c = 4$mm, $y_c = 0$ mm, $z_c = 5.2$ cm), unattenuated; and (d) off-axis ($x_c = 4$ mm, $y_c = 0$ mm, $z_c = 5.2$ cm), attenuated with 5 cm of 1.32 dB/cm/MHz. V_{pp} theory to exp. ratio = 1.102, 1.267, 0.877, and 1.041 in (a), (b), (c), and (d), respectively. V_{rms} theory to exp. ratio = 1.073, 1.255, 0.961, and 1.103 in (a), (b), (c), and (d), respectively.

segments increased the computer time from 12 to 24 min per signal determination and had less than a 1% effect on the signal amplitude and no discernible effect on the signal shape.

A. The 2.25-MHz transducer

Reference signals, the moduli of the complex $H(\omega)$ function, $|H(\omega)|$, and overlay plots of the theoretical and experimental signals for the 2.25-MHz transducer and pulsers P and U are shown in Figs. 4–6 and 7–10, respectively. For the overlay plots in these and future figures in this paper, the theory is represented by a solid line and the experiment by a broken line.

Concentrating first on the reference signals [Figs. 4(a) and 7(a)] and the moduli of the $H(\omega)$ [Figs. 4(b) and 7(b)], it is seen that the signal shapes and $|H(\omega)|$ for the two pulsers differ considerably. When pulser P was used, the peak of $|H(\omega)|$ occurred at 2.25 MHz. When pulser U was used, the peak in $|H(\omega)|$ occurred at 1.76 MHz. It should be emphasized that although the signals in Figs. 4(a) and 7(a) exhibit some similarity to the simulated pulses employed by other investigators[17-19] (damped sinusoids and sinusoids with Gaussian envelopes), the actual signal voltages cannot be fully characterized by such simple functions. The actual pressure signals corresponding to these voltage signals might more closely resemble the simulated functions, but it is again unlikely they could be fully characterized by the simulations. Finally, an additional property of the reference signals is demonstrated in Fig. 7(a). The theory and experiment are forced into agreement in the reference signal case.

In general, it is seen in Figs. 4–10 that for all cases studied, the theory and experiment are in very good agreement. This is true for various positions of the hydrophone including on- and off-axis and for both attenuated and nonattenuated pulses. Perhaps the greatest shape disagreement occurs for the unattenuated cases at or near the center of curvature of the transducer. It appears that the theoretical signals have more high-frequency structure than the experimental signals. This is confirmed in Fig. 6(b) where the moduli of the Fourier transforms of the theoretical and experimental signals are plotted. The moduli are nearly identical except in the 5.3- to 6.6-MHz frequency range where the theoretical modulus is greater than the experimental. Evidently, the $H(\omega)$ that were obtained from the signals recorded in the focal region (8 cm) of the transducer had too much high-frequency content. This may be due to the fact that the hydrophone does not behave as the flat piston receiver that was assumed. It is interesting to note that if the signal recorded at the center of curvature of the transducer is used to calculate the $H(\omega)$ for the theoretical signals, the high-frequency structure is not seen in any of the newly calculated theoretical signals, but, other than for the unattenuated signal at the center of curvature (the default reference signal case), the new theoretical results disagree more with experiment. This is true for both pulsers and both transducers. It could be concluded that a better representation of the spectral content of the pulse is obtained from reference signals recorded in the focal region rather than at the center of curvature of the transducer.

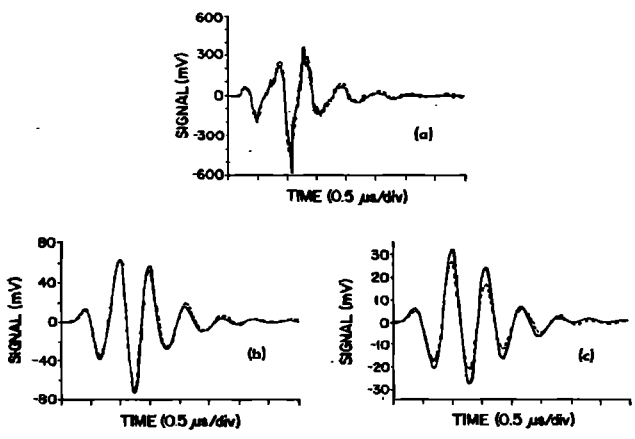

FIG. 9. 2.25-MHz transducer-pulser U results at $z_c = 13.7$ cm. Theory = solid line, experiment = broken line. (a) On-axis, unattenuated; (b) on-axis, attenuated with 5 cm of 1.32 dB/cm/MHz; and (c) off-axis ($x_c = 5$ mm, $y_c = 0$ mm, $z_c = 13.7$ cm), attenuated with 5 cm of 1.32 dB/cm/MHz. V_{pp} theory to exp. ratio = 1.379, 1.017, and 1.258 in (a), (b), and (c), respectively. V_{rms} theory to exp. ratio = 0.954, 1.030, and 1.267 in (a), (b), and (c), respectively.

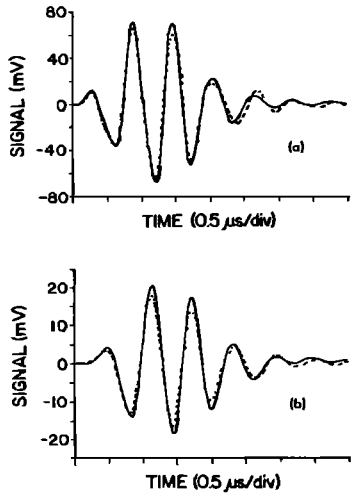

FIG. 10. 2.25-MHz transducer-pulser U results off-axis at $z_c = 18$ cm. Theory = solid line, experiment = broken line. (a) Unattenuated ($x_c = 7$ mm, $y_c = 0$ mm, $z_c = 18$ cm); and (b) attenuated with 5 cm of 1.32 dB/cm/MHz ($x_c = 7$ mm, $y_c = 0$ mm, $z_c = 18$ cm). V_{pp} theory to exp. ratio = 1.066 and 1.155 in (a) and (b), respectively. V_{rms} theory to exp. ratio = 1.076 and 1.166 in (a) and (b), respectively.

B. The 3.5-MHz transducer

Reference signals, the moduli of the hydrophone modified spectral content of these signals, and overlay plots of the theoretical and experimental signals for the 3.5-MHz transducer and pulsers P and U are displayed in Figs. 11–13 and 14 and 15. The pulser U case is of particular interest because of the unusual shape of the signal observed in the focal region of the unattenuated beam [Fig. 14(a)]. The modulus of the $H(\omega)$ correspond-

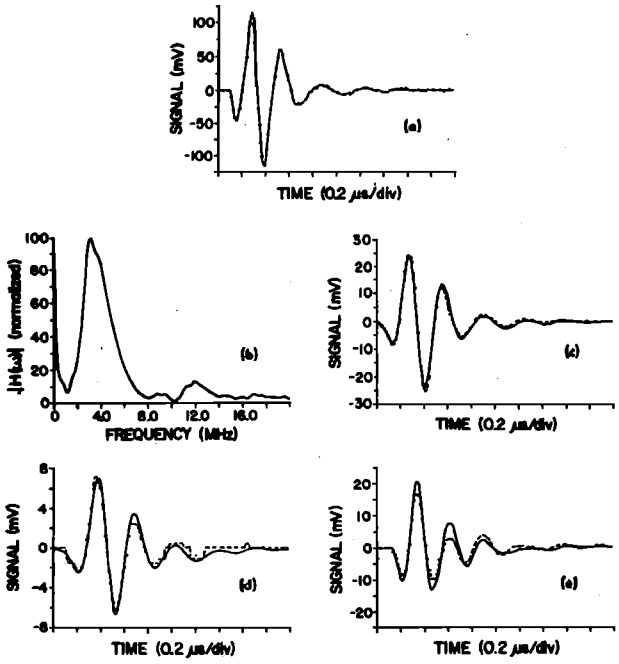

FIG. 11. 3.5-MHz transducer-pulser P results at $z_c = 8.5$ cm. Theory = solid line, experiment = broken line. (a) Reference signal—unattenuated, on-axis; (b) $|H(\omega)|$ versus frequency; (c) on-axis, attenuated with 2.52 cm of 1.32 dB/cm/MHz; (d) on-axis, attenuated with 5 cm of 1.32 dB/cm/MHz, and (e) off-axis ($x_c = 3$ mm, $y_c = 0$ mm, $z_c = 8.5$ cm) unattenuated. V_{pp} theory to exp. ratio = 0.953, 0.968, and 1.276 in (c), (d), and (e), respectively. V_{rms} theory to exp. ratio = 0.989, 1.047, 1.272 in (c), (d), and (e), respectively.

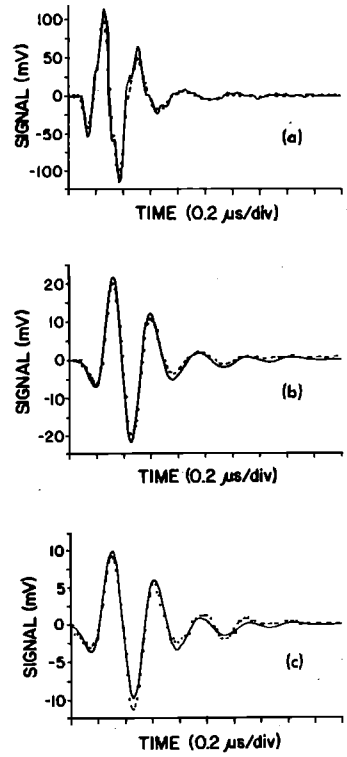

FIG. 13. 3.5-MHz transducer-pulser P results at $z_c = 10.8$ cm. Theory = solid line, experiment = broken line. (a) On-axis, unattenuated; (b) on-axis, attenuated with 2.52 cm of 1.32 dB/cm/MHz; and (c) off-axis ($x_c = 2$ mm, $y_c = 0$ mm, $z_c = 10.8$ cm, attenuated with 2.52 cm of 1.32 dB/cm/MHz. V_{pp} theory to exp. ratio = 1.194, 1.065, and 0.955 in (a), (b), and (c), respectively. V_{rms} theory to exp. ratio = 1.140, 1.076, and 1.004 in (a), (b), and (c), respectively.

ing to this signal is characterized by two peaks, one at 1.87 MHz and a second at 3.6 MHz. The unusual shape of the signal is most probably due to the manner in which the 3.5-MHz transducer responds to the excitation current pulse emitted by pulser U. However, the transient response characteristics of the hydrophone, in particular, its ring down or damping characteristics, must have played an important role in determining the signal shape. Despite the extraordinary qualities of the signal, excellent agreement between theory and experiment was obtained for all situations studied.

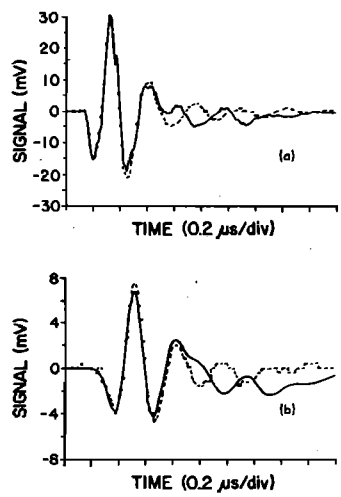

FIG. 12. 3.5-MHz transducer-pulser P results at $z_c = 3$ cm. Theory = solid line, experiment = broken line. (a) On-axis, unattenuated, (b) on-axis, attenuated with 2.52 cm of 1.32 dB/cm/MHz. V_{pp} theory to exp. ratio = 1.015 and 0.907 in (a) and (b), respectively. V_{rms} theory to exp. ratio = 0.976 and 1.085 in (a) and (b), respectively.

Two sets of comparisons in Figs. 14 and 15 deserve comment. In Figs. 14(d) and (e), two off-axis experimental signals are compared to the same theoretical signal. The experimental signals were recorded under similar conditions except, for one of the signals, the center of the hydrophone was placed at $x = 3$ mm, $y = 0$ mm, $z = 8.5$ cm; and for the other signal, the center of the hydrophone was placed at $x = -3$ mm, $y = 0$ mm, $z = 8.5$ cm. Ideally, the axial symmetry of the beam would result in the experimental signals being identical. Figures 14(d) and (e) demonstrate that there are some positioning errors or asymmetries in the ultrasonic beam associated with the experiment.

Although the beam hardening or preferential loss of high-frequency content that results from passage through the TM attenuating media is perceptible in many of the signals, it is particularly evident in a comparison of Figs. 15(a), (b), and (c). Here signals obtained at the same hydrophone position, but with 0, 2.52, and 5 cm of attenuating media between the hydrophone and transducer face, are displayed. Experiment and theory

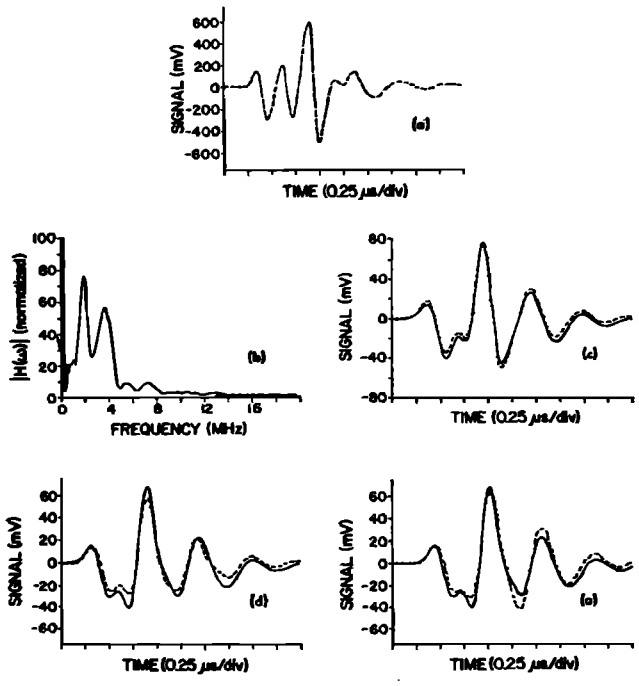

FIG. 14. 3.5-MHz transducer-pulser U results at $z_c = 8.5$ cm. Theory = solid line, experiment = broken line. (a) Reference signal—on-axis, unattenuated; (b) $|H(\omega)|$ versus frequency; (c) on-axis, attenuated with 5 cm of 1.32 dB/cm/MHz; (d) off-axis ($x_c = 3$ mm, $y_c = 0$ mm, $z_c = 8.5$ cm, attenuated with 2.52 cm of 1.32 dB/cm/MHz, and (e) off-axis ($x_c = -3$ mm, $y_c = 0$ mm, $z_c = 8.5$ cm) attenuated with 2.52 cm of 1.32 dB/cm/MHz. V_{pp} theory to exp. ratio = 0.966, 1.260, and 1.017 in (c), (d), and (e), respectively. V_{rms} theory to exp. ratio = 1.012, 1.225, and 0.976 in (c), (d), and (e), respectively.

are in very good agreement, and the increase in time between zero crossings in the waveforms that results from an increase in beam attenuation is clearly depicted.

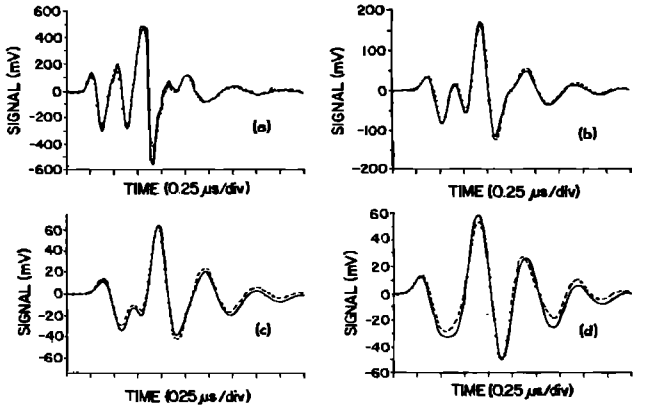

FIG. 15. 3.5-MHz transducer-pulser U results at $z_c = 10.8$ cm. Theory = solid line, experiment = broken line. (a) On-axis, unattenuated; (b) on-axis, 2.52 cm of 1.32 dB/cm/MHz attenuation; and (c) on-axis, 5-cm of 1.32 dB/cm/MHz attenuation; (d) off-axis ($x_c = 3$mm, $y_c = 0$ mm, $z_c = 10.8$ cm), 2.52 cm of 1.32 dB/cm/MHz attenuation. V_{pp} theory to exp. ratio = 1.202, 0.997, 0.983, and 1.040 in (a), (b), (c), and (d), respectively. V_{rms} theory to exp. ratio = 1.138, 1.004, 1.011, and 1.114 in (a), (b), (c), and (d), respectively.

To avoid nonlinear effects in the water–alcohol mixture when pulser P was used to excite the 3.5-MHz transducer, the pulser had to be set to emit its lowest energy pulses. Such a measure was not necessary with either transducer for pulser U or with the 2.25-MHz transducer for pulser P because the spectral distributions of the resulting pressure waves were more weighted toward the low frequencies. As shown in Figs. 11–13, the low energy 3.5-MHz transducer-pulser P signals were of a much more regular shape than the 3.5-MHz transducer-pulser U signals, and the $|H(\omega)|$ of the former was also of a more usual shape with a single dominant peak at 3.12 MHz. The model performed quite well. The stairstep-like nature of some of the experimentally obtained attenuated signals relates to the fact that the signals were so small that only a fraction of the full-scale 8-bit resolution of the transient recorder was effectively employed in their digitization. The signals in Fig. 12 correspond to a closer axial position than previously examined, 3 cm. A feature of these signals which was not exhibited in the other studies is the nearly 180° out-of-phase relationship between the final cycles of the theoretical and experimental pulses. It is believed that this incongruity is due to a characteristic of the hydrophone that was not modeled. There is a butyl rubber collar on the front of the hydrophone and it most likely blocked the reception of some of the beam originating from the edges of the transducer. A more detailed analysis is included in the edge wave section of this paper.

IV. DISCUSSION

As with the 2.25-MHz transducer signals, it is highly unlikely that the 3.5-MHz transducer signals could be adequately represented by any of the common simulations. This is especially true in the case of the signals obtained with pulser U.

It is interesting to note that the theoretical 3.5-MHz transducer results, in general, agreed better with experiment than the theoretical 2.25-MHz transducer results. One could conclude that the 3.5-MHz transducer was better characterized by the model that was employed.

A. Nonlinear effects

It was possible to introduce clear evidence of nonlinear effects generated in the water/alcohol mixture when a pulse from pulser P of greater energy than that discussed above was used to excite the 3.5-MHz transducer. Such effects were also observed in the beam generated by the 3.5-MHz transducer when it was pulsed by a more up-to-date commercial B-scan ultrasound machine. This instrument is currently used to scan patients in a hospital clinic, and the nonlinear effects in the water/alcohol mixture occurred when the voltage pulser on the unit was set at a level commonly used in patient examinations. Thus the high energy pulser P results have clinical relevance.

The unattenuated reference signal recorded by the hydrophone in the focal region of the 3.5-MHz transducer when it was pulsed with a higher amplitude voltage

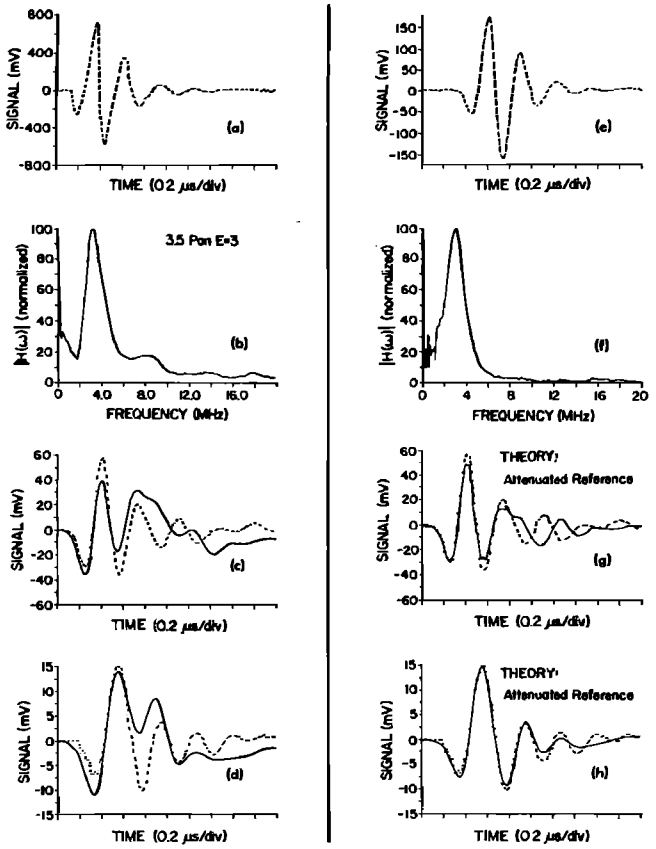

FIG. 16. Nonlinear effects study. 3.5-MHz transducer-pulser P with high intensity pulses. Theory = solid line, experiment = broken line. (a) Reference signal—unattenuated, on-axis, z_c = 8.5 cm; (b) $|H(\omega)|$ versus frequency for reference signal in (a). The corresponding $H(\omega)$ are used to calculate the theoretical signals in (c) and (d); (c) theory versus experiment: on-axis, z_c = 3 cm, 2.52 cm of 1.32 dB/cm/MHz attenuation; (d) theory versus experiment; off-axis (x_c = 3 mm, y_c = 0 mm, z_c = 10.8 cm) 2.52 cm of 1.32 dB/cm/MHz attenuation; (e) attenuated reference signal—on-axis, z_c = 8.5 cm, 2.52 cm of 1.32 dB/cm/MHz; (f) $|H(\omega)|$ versus frequency for reference signal in (e). The corresponding $H(\omega)$ are used to calculate the theoretical signals in (g) and (h); (g) theory versus experiment: same conditions as in (c) but reference signal in (e) is used in the theory; and (h) theory versus experiment: same conditions as in (d), but reference signal in (e) is used in the theory.

spike from pulser P is displayed in Fig. 16(a). The downward slope of the second half-cycle of the signal is much steeper than that of the lower energy signal shown in Fig. 11(a). This is a characteristic of the distorted waveform that can result from nonlinear effects as described in a recent article by Muir and Carstensen.[27] The distortion arises from the compressional phase of a high intensity waveform having greater speed than the rarefaction phase. Further evidence of nonlinear effects is obtained when an estimate of the intensity of the high energy reference signal is made. Using a K_f^2 value for the hydrophone of 43.8×10^{-4} $V^2/W/cm^2$ (Ref. 28) at f = 3.32 MHz (which is the peak value of the modulus of the Fourier transform of the reference signal) and letting V equal one-half the peak-to-peak voltage (V = 0.64 V), the peak intensity can be estimated to be 93.5 W/cm^2. This is definitely in the nonlinear region as shown in the Muir and Carstensen article.

Since the superposition theory for pulsed waveforms from a focused radiator assumes a linear system, it would be expected to fail for nonlinear signals. This is evident in the comparisons between theory and experiment shown in Figs. 16(c) and (d).

If an attenuating phantom is placed between the transducer and the hydrophone so as to reduce the energy of the pressure pulse that gives rise to the reference signal, the improvement in agreement between experiment and theory is dramatic. The results of such a study involving the same experimental signals as those shown in Figs. 16(a), (c), and (d) are shown in Figs. 16(e), (g), and (h). For this particular case, the $H(\omega)$ were obtained from an experimental signal which was output by the hydrophone when it was placed in the focal region of the transducer, behind a 2.52 cm thick phantom of attenuating media. The fact that this signal was attenuated was accounted for in the theoretical calculations by assuming phantom thicknesses of 0 and 2.48 cm for the cases in which the experimental signals had actually been obtained through 2.52 and 5 cm thick phantoms, respectively. Plots of the moduli of the $H(\omega)$ for the nonlinear reference signal (z = 8 cm, unattenuated) and the attenuated reference signal are shown in Figs. 16(b) and (f). In the nonlinear case, the modulus of $H(\omega)$ in the 6–9-MHz region is approximately 17% of the peak spectral value; whereas in the attenuated case, this modulus is ~2%–3% of the peak spectral value. Since ultrasonic transducers are designed to have a thickness equal to one-half the wavelength of their desired resonant frequency,[29] second harmonics emitted by such transducers are normally of a negligible magnitude. Nonlinear effects do give rise to the generation of harmonics in a pressure waveform; hence, they would be the suspected cause of the 6–9-MHz peak in the spectrum of the unattenuated reference signal, which corresponds to the second harmonic of the 3–4.5-MHz peak.

In summary, if the experimental signal level is large enough that significant nonlinear effects occur during transmission of the pulse through the region of space (volume) investigated, the theory will be in error. However, in these cases, it is possible to reduce the pulse amplitude using attenuating material, producing a waveform for which the present theory is applicable.

B. The effects of different dispersion relations

The importance of the frequency dependence of the speed of sound or the dispersion relations on the signal shape were investigated by comparing plots acquired when different dispersion relations were input into the theory. A comparison between theory and experiment depicting the effects of these relations for the case of the signal obtained on-axis at z = 15 cm after passing through a 5 cm thick phantom of attenuating media for the 3.5-MHz transducer-pulser U combination is shown in Fig. 17. In 17(a), the measured dispersion relation [Eq. (14)] was input into the theory; in 17(b), only the Kramers–Kronig relation was input; and in 17(c), the speed of sound was assumed to be 1570 m/s independent of frequency. As might be expected, the theory agreed

best with experiment in 17(a). Disagreement between theory and experiment at the beginning of the signal is evident in 17(b) and even more so in 17(c). It appears that a fairly adequate representation of the signal can be predicted if only the Kramers–Kronig dispersion relation is employed in the theory. Even for the constant speed of sound case, the general waveform, peak-to-peak and rms values are still in relatively good agreement with the experiment. However, greater disparity would be expected for cases in which the hydrophone were positioned at a greater distance from the transducer face and a greater amount of attenuation were placed in the beam.

C. The existence of edge waves

Kaspar'yants[2] and Kozina and Makarov[3] first described pulses emanating from piston radiators in terms of a plane-wave component radiated by the whole transducer plus a diffracted-wave component originating from the edge of the transducer. Tupholme[5] has termed these components direct and edge waves. Using a 150-μm diam omnidirectional hydrophone, Weight and Hayman[15] observed edge and direct waves on axis emanating from a pulsed circular piston transducer, and found that they compared favorably to those predicted using an unpublished theoretical expression derived by Duck.[15] Such waves would also be expected to emanate from pulsed focused radiators. As discussed previously, the hydrophone that was employed in our experimental studies had a rubber collar that extended beyond the active element. This collar likely blocked the reception of the edge waves, especially when the hydrophone was positioned close to the transducer face. As shown in Fig. 12, the experimental signal obtained on-axis at $z = 3$ cm does not show any evidence of edge waves, but the theoretical signal does. The tail end of the theoretical signal exhibits the results of the merging of the direct and edge waves. This was only observed in the theoretical calculations because the rubber collar on the hydrophone was not included in the hydrophone model.

Due to the fact that the pressure waves from all points on the transducer face are in phase at the center of curvature of the transducer, the signal detected by a point receiver placed at this position would be expected to be very similar to that detected by the 0.75-mm radius hydrophone. Therefore the results for a point receiver can be simulated by assuming in the model that a reference signal obtained with the hydrophone at the center of curvature was actually obtained with a point receiver. A study of this nature was performed, and the predicted waveforms at various axial positions are shown in Fig. 18. At $z = 1$ cm [Fig. 18(a)], the edge and direct waves are clearly discernible. The direct wave corresponds to the pulse on the left in Fig. 18(a), and the edge wave is the inverted replica of the direct wave which corresponds to the pulse on the right. The time delay between the two pulses is determined by the difference between the distance from the observation point to the center of the transducer and the distance from the observation point to the edge of the transducer. As the axial distance of the observation point is increased (Fig. 18), the edge pulse and the direct pulse merge into one pulse. All of these observations are consistent with results published by Weight and Hayman[15] and Rob-

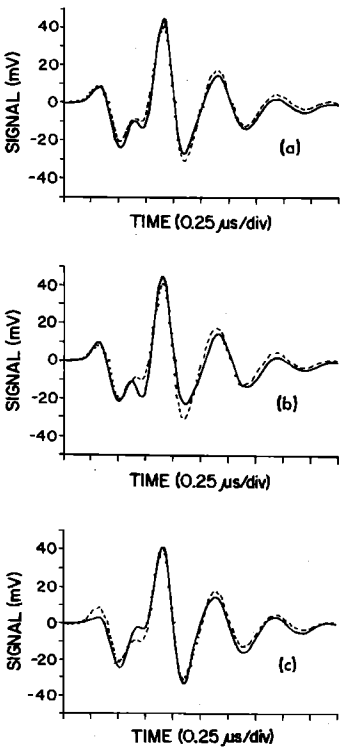

FIG. 17. Dispersion relation study. 3.5-MHz transducer-pulser U. On-axis, $z_c = 15$ cm, 5 cm of 1.32-dB/cm/MHz attenuation. Theory = solid line, experiment = broken line. (a) Theory—measured $c(\omega)$; (b) theory—Kramers–Kronig $c(\omega)$ only; and (c) theory—$c(\omega)$ = constant 1570 m/s. V_{pp} theory to exp. ratio = 0.995, 0.951, and 1.047 in (a), (b), and (c), respectively. V_{rms} theory to exp. ratio = 1.019, 1.018, and 1.018 in (a), (b), and (c), respectively.

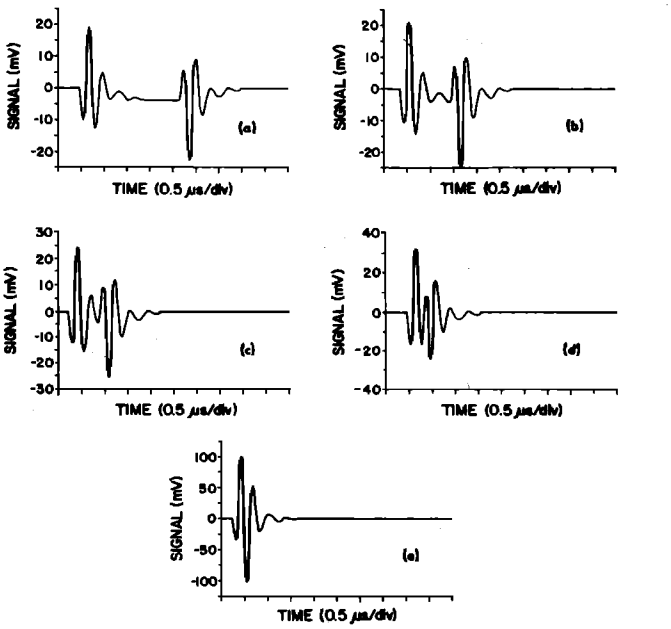

FIG. 18. Edge wave study (theory). 3.5-MHz transducer-pulser P, assumed point receiver, unattenuated signals. (a) On-axis, $z = 1$ cm; (b) on-axis, $z = 2$ cm; (c) on-axis, $z = 3$ cm; (d) on-axis, $z = 5$ cm, and (e) on-axis, $z = 8.5$ cm.

inson *et al.*[12] In summary, it is possible to show that for the focused radiator, the pressure pulses may be described, as in the piston radiator case, in terms of direct and edge waves.

V. CONCLUSIONS

The good agreement between theory and experiment shown in Figs. 4–10 and 11–15 proves the utility of the model which was implemented in this paper to predict the field patterns of pulsed, focused radiators in both attenuating and nonattenuating media. Reasons for the small discrepancies that are sometimes observed probably relate most to nonideal or unmodeled behavior of the transducer and the hydrophone and experimental positioning errors.

As was pointed out in the companion article,[20] the continuous wave theory breaks down in the region very near (~1 cm from) the radiator. Since the pulse theory utilizes a superposition of many continuous wave sinusoids to form the pulsed signal, it too must break down in this region. Also, because the theory is dependent upon linearity, it fails in cases in which nonlinear effects are appreciable. However, if the high-intensity pulses associated with these nonlinear effects are attenuated enough prior to the recording of the reference signal, the theory can be successfully used to predict the experimental signals.

The single integral aspect of the theory results in considerable savings of computer time. In the studies reported in this paper, a Gaussian quadrature numerical integration scheme of order $n = 96$ was employed to calculate the single integral. Had double integration of the same order been used, the amount of computer time involved would have increased by a factor of at least 48. That is, a single signal would have been calculated by the minicomputer in 9.6 h instead of 12 min.

It should be reiterated that voltage signals output by the hydrophone rather than pressure or force signals were compared in this paper. It was shown that this was adequate for testing the theory. Integrated pressure (force) signals could be obtained from these voltage signals if the force-to-voltage transfer characteristics of the hydrophone at all of the frequencies involved in the pulse were known. With the transfer function in hand, future applications of this theory to ultrasonic dosimetry might be explored.

ACKNOWLEDGMENTS

The authors wish to thank Barbara Goodsitt for assisting in the preparation of the figures in this paper and Anne Zimmerman for typing the manuscript. We also wish to thank Richard Banjavic and Paul Carson for lending us the hydrophone that we used in the experimental studies. This work was supported in part by NCI grants # 5-T32-CA09206, 5-R01-CA25634, and 5-P01-CA19278.

[1]R. Kuc, M. Schwartz, and L. Von Micsy, "Parametric Estimation of the Acoustic Attenuation Coefficient Slope for Soft Tissue," IEEE Ultrason. Symp. Proc., Cat. No. 76 CH 1120-5SU, 44–47 (1976).
[2]A. A. Kaspar'yants, "Non-stationary Radiation of Sound by a Piston," Akust. Zh. 6, 52–56 (1960). [Engl. transl.: Sov. Phys.-Acoust. 6, 39–43 (1960).]
[3]O. G. Kozina and G. I. Makarov, "Transient Processes in the Acoustic Fields Generated by a Piston Membrane of Arbitrary Shape," Akust. Zh. 7, 53–58 (1961). [Engl. transl.: Sov. Phys.-Acoust. 7, 53–58 (1961).]
[4]F. Oberhettinger, "On Transient Solutions of the Baffled Piston Problem," J. Res. Natl. Bur. Stand. 65B, 1–6 (1961).
[5]G. E. Tupholme, "Generation of Acoustic Pulses by Baffled Plane Pistons," Mathematika 16, 209–224 (1969).
[6]L. Bess, "Sonic Radiation from a Circular Piston with Impulse Excitation," NASA Electron. Res. Cent., Cambridge, MA Informal Rep. (April 1970) (unpublished).
[7]A. Freedman, "Transient Fields of Acoustic Radiators," J. Acoust. Soc. Am. 48, 135–138 (1970).
[8]A. Freedman, "Sound Field of Plane or Gently Curved Pulsed Radiators," J. Acoust. Soc. Am. 48, 221–227 (1970).
[9]A. Freedman, "Farfield of Pulsed Rectangular Acoustic Radiators," J. Acoust. Soc. Am. 49, 738–748 (1971).
[10]P. R. Stephanishen, "Transient Radiation from Pistons in an Infinite Planar Baffle," J. Acoust. Soc. Am. 49, 1629–1638 (1971).
[11]A. Freedman, "Soundfield of a Pulsed, Planar, Straight-edged Radiator," J. Acoust. Soc. Am. 51, 1624–1639 (1972).
[12]D. E. Robinson, S. Lees, and L. Beso, "Near Field Transient Radiation Patterns for Circular Pistons," IEEE Trans. Acoust., Speech, Signal Process. ASSP-22, 395–403 (1974).
[13]W. L. Beaver, "Sonic Nearfields of a Pulsed Piston Radiator," J. Acoust. Soc. Am. 56, 1043–1048 (1974).
[14]M. Auphan and H. Dormant, "Pulsed Acoustic Radiation of Plane Damped Transducers," Ultrasonics 15, 159–168 (1977).
[15]J. P. Weight and A. J. Hayman, "Observations of the Propagation of Very Short Ultrasonic Pulses and Their Reflection by Small Targets," J. Acoust. Soc. Am. 63, 395–404 (1978).
[16]J. Engelbrecht and R. C. Chivers, "The Sound Field of Pulsed Ultrasonic Transducers Described by Evolution Equations," Acoust. Lett. 3, 120–123 (1979).
[17]A. Weyns, "Radiation Field Calculations of Pulsed Ultrasonic Transducers: Part 1—Planar Circular, Square and Annular Transducers," Ultrasonics 18, 183–188 (1980).
[18]B. Bardsley and D. Christensen, "Beam Patterns from Pulsed Ultrasonic Transducers Using Linear Systems Theory," J. Acoust. Soc. Am. 69, 25–30 (1981).
[19]A. Weyns, "Radiation Field Calculations of Pulsed Ultrasonic Transducers: Part 2—Spherical Disc- and Ring-shaped Transducers," Ultrasonics 18, 219–223 (1980).
[20]E. Madsen, M. Goodsitt, and J. Zagzebski, "Continuous Waves Generated by Focused Radiators," J. Acoust. Soc. Am. 70, 1508–1517 (1981).
[21]H. T. O'Neil, "Theory of Focusing Radiators," J. Acoust. Soc. Am. 21, 516–526 (1949).
[22]C. E. Shannon and W. Weaver, *The Mathematical Theory of Communication* (Univ. Illinois P., Urbana, 1949).
[23]E. T. Whittaker, "Expansion of the Interpolation Theory," Proc. R. Soc. Edinburgh 35, 181 (1915).
[24]P. T. Wilson, R. H. Tancrell, and J. Callerane, "PVF_2 Polymer Microprobe," 1979 Ultrason. Symp. Proc., IEEE 79CH1482-9SV (1979).
[25]E. Madsen, J. Zagzebski, R. Banjavic, and R. Jutila, "Tissue Mimicking Materials for Ultrasound Phantoms," Med. Phys. 5, 391–394 (1978).
[26]M. O'Donnell, E. T. Jaynes, and J. G. Miller, "Kramer–Kronig Relationship Between Ultrasonic Attenuation and Phase Velocity," J. Acoust. Soc. Am. 69, 696–701 (1981).
[27]T. G. Muir and E. L. Carstensen, "Prediction of Nonlinear Acoustic Effects at Biomedical Frequencies and Intensities," Ultrasound in Med. and Biol. 6, 345–357 (1980).
[28]R. A. Banjavic, Univ. Colorado (personal communication).
[29]P. N. T. Wells, *Biomedical Ultrasonics* (Academic, New York, 1977), Chap. 3, p. 53.